Electronic Supplementary Information

Mitochondria-targeted Fluorophores for in vivo NIR-II Imaging-guided PDT/PTT

Qihang Ding[a,‡], Ling Mei[c,‡], Yu Liu[b,‡], Shan Zhou[b], Lu Chen[b], Yuying Liang[b], Mingle Li[a], Hui Zhou[b,*], Chao Yin[b,*] and Jong Seung Kim[a,*]

[a] *Department of Chemistry, Korea University, Seoul 02841, Korea. E-mail: jongskim@korea.ac.kr*
[b] *State Key Laboratory of Organic Electronics and Information Displays & Institute of Advanced Materials (IAM), Nanjing University of Posts & Telecommunications, 9 Wenyuan Road, Nanjing 210023, China. E-mail: iamhzhou@njupt.edu.cn; iamcyin@njupt.edu.cn*
[c] *Engineering Research Center for Pharmaceuticals and Equipment of Sichuan Province, Sichuan Industrial Institute of Antibiotics, School of Pharmacy, Chengdu University, Chengdu 610106, China.*
‡ These authors contributed equally to this work

Materials and characterization

All chemicals were purchased from commercial sources (such as Aldrich, Energy Chemical, TCI) and used without further purification unless otherwise noted. Compound 1 was purchased from WuXi AppTec. The synthetic procedures have been reported in previous referecens.[1,2] MALDI-TOF-MS characteristics were performed on Bruker, autoflex speed Maldi-Tof. The absorption data was measured by a Shimadzu UV-3600 ultraviolet-visible-near infrared spectrophotometer. NIR-II spectrophotometer (Fluorolog 3, Horiba) equipped with an 808 nm diode laser. NIR-II fluorescence imaging was conducted on a NIR-II imaging system (Wuhan Grand imaging Technology Co., Ltd). Transmission electron microscopy (TEM) imaging was performed by using an HT7700 transmission electron microscope operating at an acceleration voltage of 100 kV. Confocal fluorescence images were captured on the confocal laser scanning microscope (CLSM) with a two-photon in vivo imaging microscope (Zeiss optical instruments International Trading Co., Lt) and Leica SPE. Schematic illustration was created by Biorender.

Experimental sections

NIR-II Fluorescence Imaging Depth. MTF solution (dissolved in DMSO) was added to the 96-well plates. Then, the chicken breast with various thickness covered the wells. The fluorescence images were acquired under 808 nm laser excitation, and the exposure time was set as 50 ms.

Extracellular ROS detection. The generation of extracellular ROS was measured with a DPBF probe. Briefly, different concentrations of MTF (10 μM, containing 100 μl EtOH solution) were added into 3 mL of ethanol solution containing DPBF (10 mM), and then the solution was kept in the dark to avoid interference and irradiated

by an 808 nm laser continuously for various time periods (0, 20, 40, 60, 80, 100 seconds). The spectrum was collected at 415 nm absorption.

ROS Measurement in 4T1 Cells 4T1 cells (1×10^4 cells/well) were seeded into a 96-well plate and incubated with MTF (10 nM or 20 nM) for 6 h and 1 μM DCFH-DA for 30 min. The cells were then exposed to laser irradiation (1 W/cm^2, 808 nm) for 1 min prior to imaging. To visualize ROS generation under various conditions, every well was visualized under an inverted fluorescence microscope.

Cell Culture and Cytotoxicity Assay. Cell viability was measured using the CCK-8 assay according to the manufacturer's instructions. The 4T1 cells were seeded at a density of 1×10^4 per well (100 μL total volume per well) in 96-well assay plates. After 24 h incubation, the medium was replaced by a fresh medium containing different concentrations of MTF (0, 5, 10, 20, 40 nM) and incubated for an additional 8 h. Then, an 808 nm laser (0.5 W/cm^2) was used to irradiate cells for 2 min, and cells were continued to incubate for 12 h. Afterward, the cell viability was evaluated using a CCK-8 kit.

Calcein-AM/ PI staining of live/dead cells. The 4T1 cells were seeded at a density of 1×10^4 per well (100 μL total volume per well) in 96-well assay plates. After 24 h incubation, the medium was replaced by a fresh medium containing 20 nM of MTF and incubated for an additional 6 h. Then, an 808 nm laser (0.5 W/cm^2) was used to irradiate cells for 3 min. After that, cells were replaced with fresh DMEM medium and cells were continued to incubate for 8 h. Afterward, the cells were stained using Calcein-AM/ PI kit.

Preparation and Characterization of MTF dots. MTF (1 mg) was dissolved in 1 mL THF, and DSPE-PEG2k (9 mg) was completely dissolved in water (9 mL) to obtain DSPE-PEG2k solution. Then the MTF solution was added dropwise into DSPE-PEG2k solution under strong sonication. After 5 min sonication, the organic solvent was removed under N_2 flow, then the resulting mixture was washed several times using a 30 kDa centrifugal filter unit and concentrated to yield **MTF dots**. The resulting **MTF dots** was stored in dark at 4 ^{o}C for further usage.

***In vivo* NIR-II fluorescence imaging.**

All the mice experiments were conducted in accordance with the guidelines of the Laboratory Animal Center of Jiangsu KeyGEN Biotech Corp., Ltd and approved by the Animal Ethics Committee of Simcere BioTech Corp., Ltd. The mice were anesthetized using isoflurane if necessary. Male BALB/c mice (4 weeks old, ~20 g body weight) were injected 4T1 cells subcutaneously in the right flank region with 200 μL of cell suspension containing 5×10^6 4T1 cells. The tumors were allowed to grow to ~200 mm^3 before experiments. The mice were intravenously injected with **MTF dots** (200 μL, 1 mg/mL) and then imaged at different time points of post-injection (6, 12, 24, 36, 48, 60 h) under 808 nm laser excitation, and the exposure time was set as 300 ms. The mice were sacrificed at 60 h i.v. post-injection. The major organs including tumors were also collected under 808 nm laser at the exposure time of 350 ms.

In vivo Photodynamic Therapy. 4T1 tumor models were established using the abovementioned method. Mice were randomly divided into 4 groups (n=5 each) and monitored until tumor volumes reached *ca*. 100 mm^3. The mice were treated with either PBS (200 μL) or MTF dots (200 μL, 2000 μg/mL) w/o irradiation (808 nm, 1.2 W/cm^2, 6 min). After treatment, the weight and tumor volumes of each mouse were recorded every other day for 22 d.

Photothermal performance measurement. The temperature curve over time was plotted through employing an infrared thermal camera (FORTRIC 225) to record the temperature variation in **MTF**(80 μM, 100 μM) and **MTF dots** (100 μg/ml, 150 μg/ml) with different concentration under 808 nm laser irradiation (1 W cm^{-2} , 10 min). The photothermal conversion efficiency (η) of **MTF dots** was calculated according to the equation as follows in previous report:[2]

$$\eta = \frac{hS\Delta T_{max} - Q_S}{I(1 - 10^{-A808})}$$

where, h represents the heat transfer coefficient, S is the surface area of the container, ΔT_{max} represents the largest temperature difference that occurs between the maximum steady-state temperature and the ambient temperature of the surrounding environment, Qs represents the heat associated with the light absorbance of water, I is the laser power density, and A808 is the absorbance of **MTF dots** at 808 nm. and hS = mc/τ. m represents the solution mass, c means the specific heat capacity of water, 4.2×10^3 J /(kg·°C), and τ is acquired from the cooling process and time.

In vivo photothermal imaging. Male Balb/c 4T1 mice bearing tumors were administered intravenous injections of **MTF dots** (200 μL, 1 mg/mL). After 24 hours, the mice were anesthetized with an intraperitoneal injection of pentobarbital sodium solution (50 mg kg^{-1}), and the tumor was exposed to 808 nm laser radiation (1 W cm^{-2}) for 6 minutes. The resulting temperature changes in the tumor were recorded using an IR thermal camera during the 6-minute irradiation period to evaluate the photothermal effects of the **MTF dots**.

Quantum yield. To determine the quantum yield of **MTF dots**, IR-26 (with a quantum yield of 0.5%) was selected as a reference compound.[4] The fluorescence of **MTF dots** and IR-26 was measured at five different concentrations, and the integrated fluorescence of the 1000-1400 nm region was plotted against the absorbance at the excitation wavelength of 808 nm. By comparing the slopes of these plots, the quantum yield of **MTF dots** was determined. The quantum yield of **MTF dots** was calculated using the following formula:

$$QY_{sam} = QY_{ref} \times \frac{S_{sam}}{S_{ref}} \times \left(\frac{n_{sam}}{n_{ref}}\right)^2$$

Where QY_{sam} is the quantum yield of MTF dots in water, QY_{ref} is the quantum yield of IR-26 (~ 0.5%) in DCE, S_{sam} and S_{ref} are the slopes obtained by linear fitting of the integrated fluorescence intensity of **MTF dots** (1000-1400 nm) and IR-26 (1000-1400 nm) against the absorbance at 808 nm. n_{sam} and n_{ref} are the refractive indices of their respective solvents (Serum ≈ Water: 1. 333 and DCE: 1.444).

ROS quantum yield. For this experiment, **MTF, MTF dots** and ICG were dissolved in DMF and water respectively to achieve an absorption of 0.5-0.9 OD at 808 nm, and DPBF was added to a concentration of 80 μM. The solutions were then exposed to an 808 nm laser at 1 W cm^{-2}, while their UV-Vis spectra and absorption intensities at 415 nm were recorded every 30 seconds using a spectrophotometer. The decrease in DPBF absorption intensity at 415 nm was plotted for **MTF**, **MTF dots** and ICG, and their respective ROS quantum yields (ΦΔ) were calculated using the following formula:[3]

$$\Phi\Delta = \Phi_{ICG} \times \frac{K_{PS} \times F_{ICG}}{K_{ICG} \times F_{PS}}$$

The ROS quantum yield of **MTF** and **MTF dots** (ΦΔ) and the ROS quantum yield of ICG in water (Φ_{ICG}) were determined, based on a reference.[3] The slope (k) was obtained through linear regression of the decrease in DPBF absorption intensity, while the absorption correction factor (F) was calculated using the formula $F = 1\text{-}10^{OD}$, with

OD representing the absorption at the irradiation wavelength(808 nm).

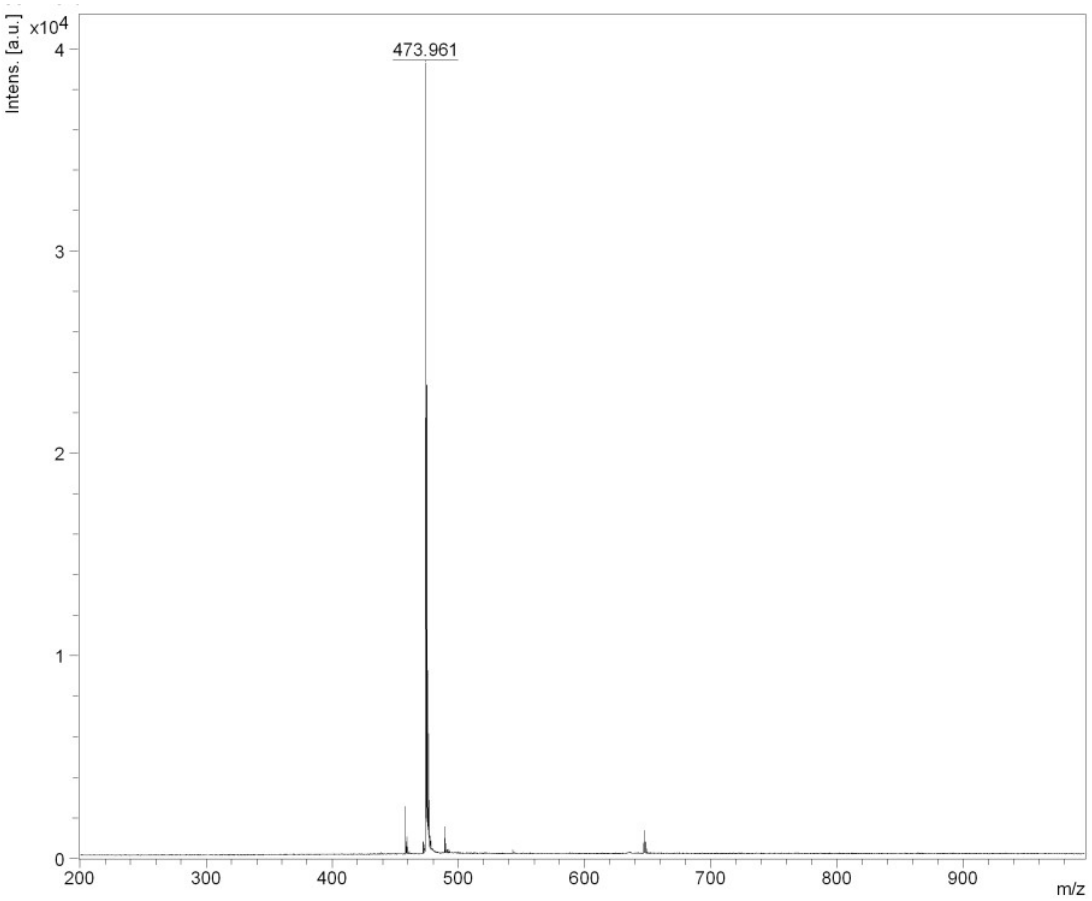

Fig. S1 MALDI-TOF-MS Spectrum of **MTF**. Expected M.W.474.188, Measured M.W. 473.961.

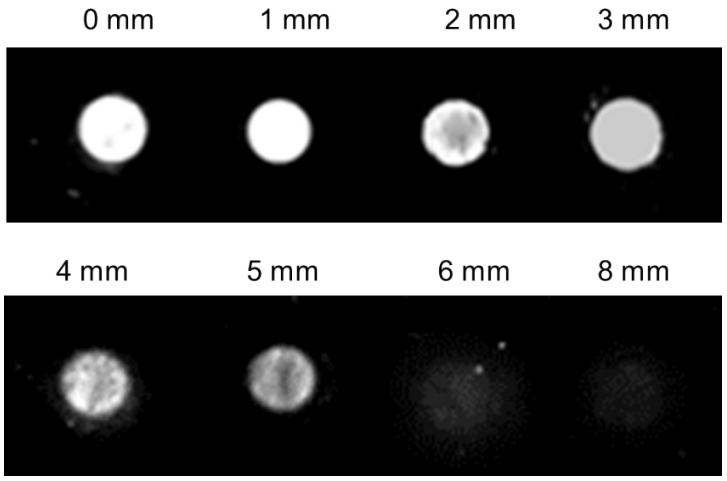

Fig. S2 NIR-II fluorescence of **MTF** covered by chicken breast tissue with different thicknesses.

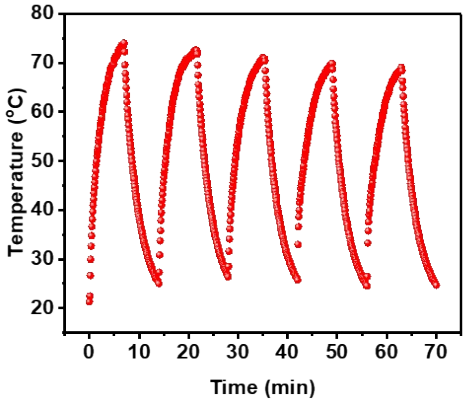

Fig. S3 The photothermal stability of **MTF** (100 μg/mL) evaluated by five photoirradiation–cooling cycles (808 nm, 1 W/cm^2).

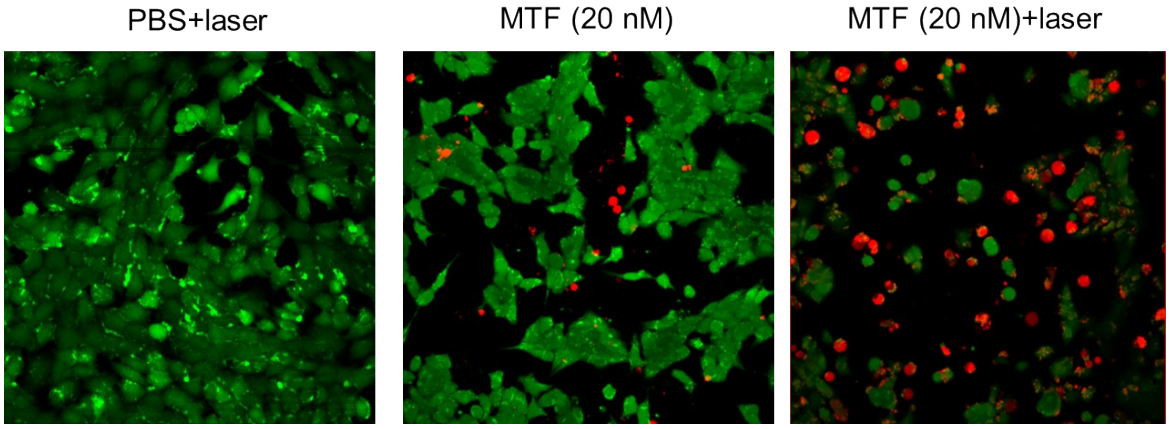

Fig. S4 Live/dead staining of 4T1 cells received different treatments.

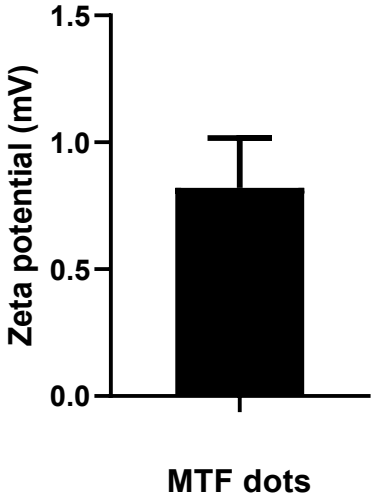

Fig. S5 Zeta potential of **MTF dots.**

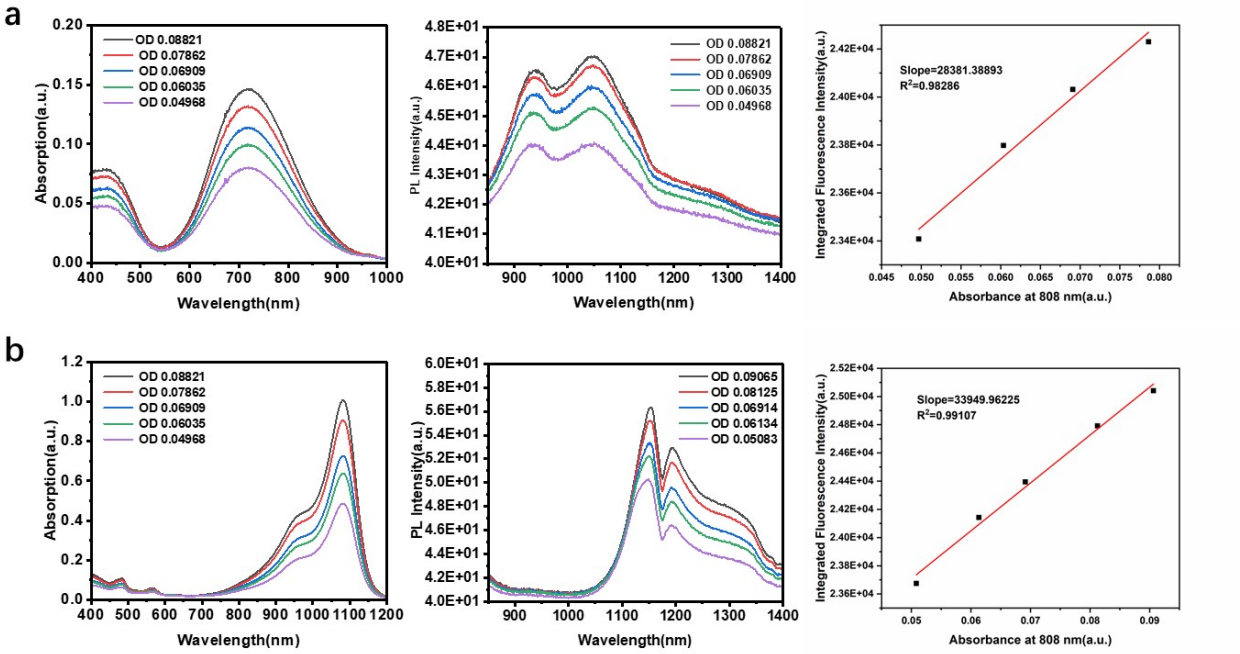

Fig. S6 . (a) Quantum yield measurements of **MTF dots** in water. (b) IR-26 in DCE was chosen as a reference.

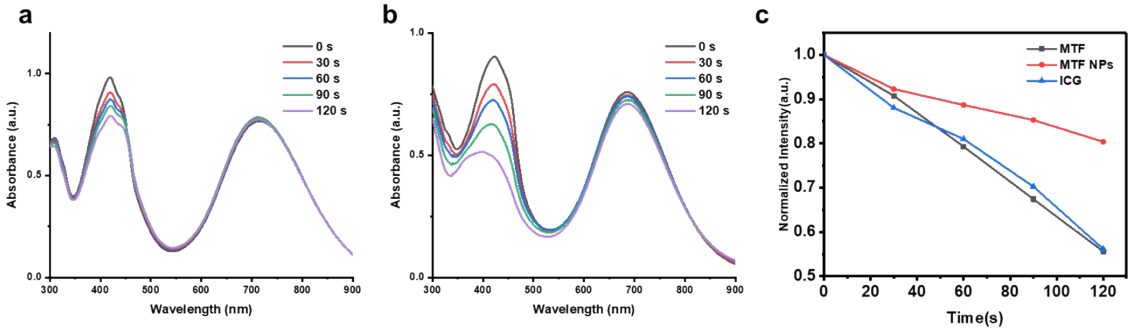

Fig. S7 (a) The absorption spectrums of DPBF for **MTF dots** and (b) ICG upon different irradiation time (808 nm, 1 W/cm^2). (c) The corresponding linear fitting of the decreased absorption intensity of DPBF.

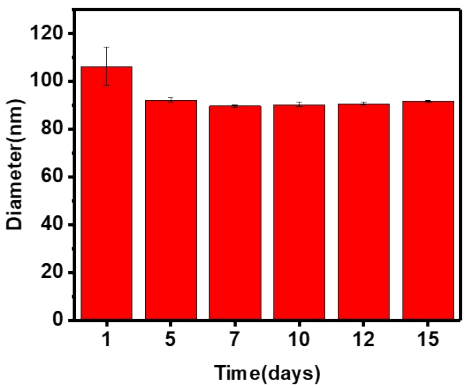

Fig. S8 The size stability of **MTF dots** (150 μg/mL)in water for 15 days.

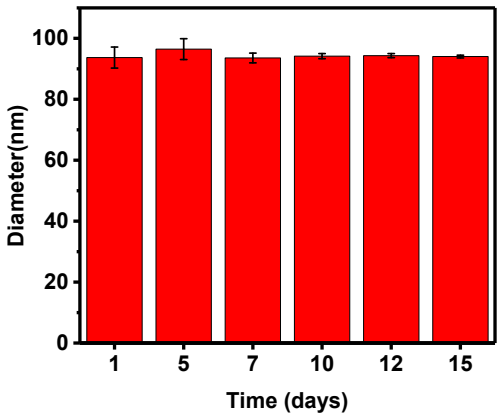

Fig. S9 The size stability of **MTF dots** (150 μg/mL)in DMEM for 15 days.

Fig. S10 Photostability of **MTF dots** and ICG in water under laser irradiation (808 nm, 1W/cm^2).

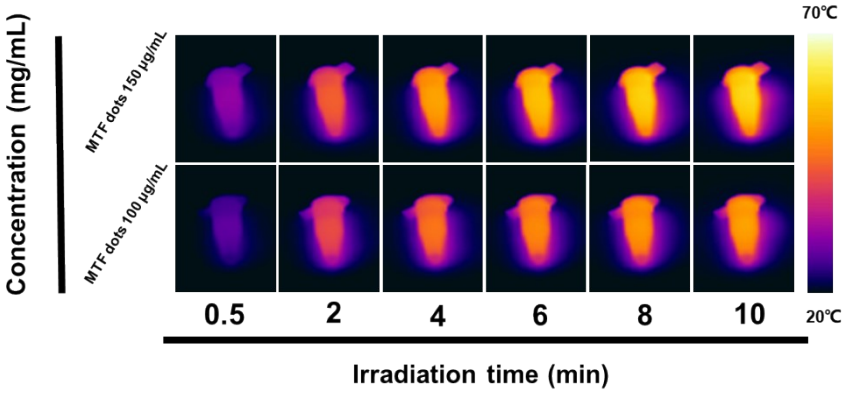

Fig. S11 IR thermal photos of **MTF dots** (100 and 150 μg/mg) in the DMF under 808 nm laser irradiation (1 W/cm^2).

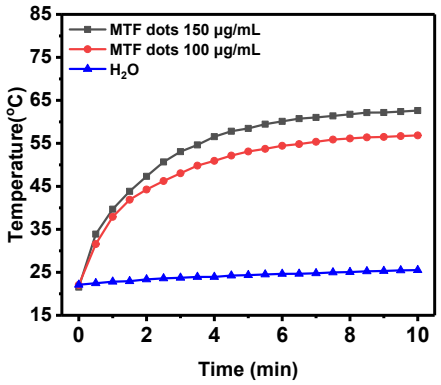

Fig. S12 Temperature change curves of **MTF dots** (100 and 150 μg/ml) under the laser irradiation (808 nm, 1 W/cm^2) at various concentrations.

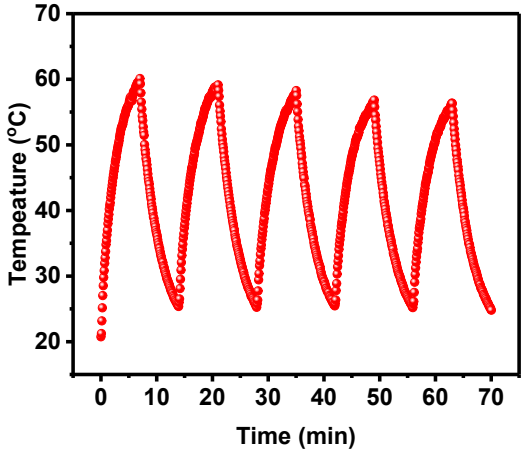

Fig. S13 The photothermal stability of **MTF dots** (150 μg/mL) evaluated by five photoirradiation–cooling cycles (808 nm, 1 W/cm^2).

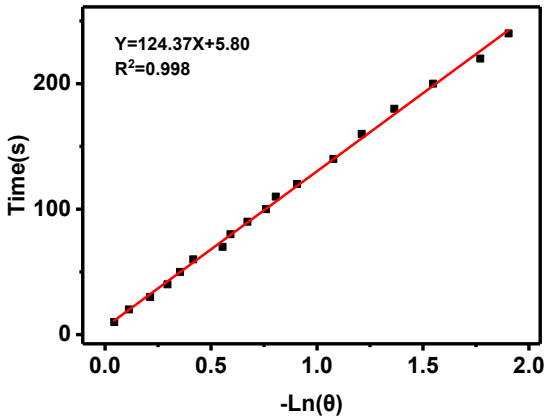

Fig. S14 Calculation of the photothermal conversion efficiency (808 nm, 1.0 W/cm^2). Red line: Linear time data *versus* −ln θ during the cooling period.

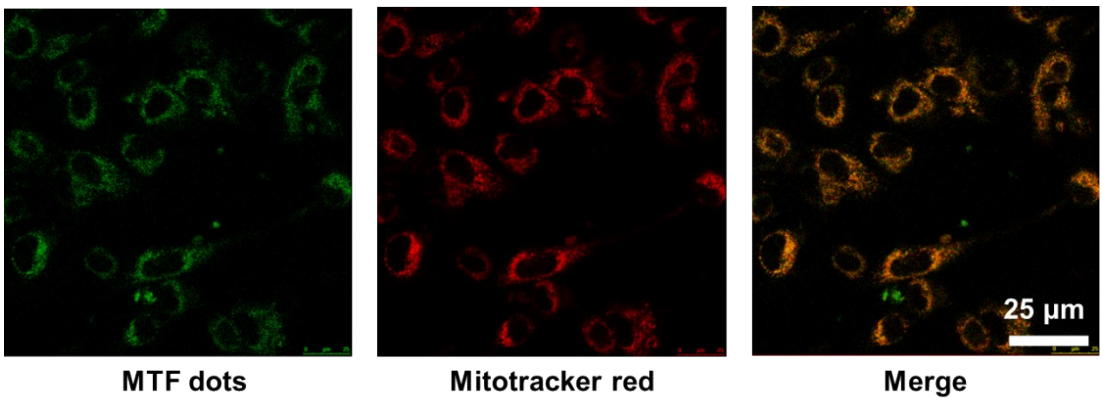

Fig. S15 Mitochondiral colocalization assay of **MTF dots** (50 μg/mL, 6 h) in 4T1 cells. λem: 490–530 nm (**MTF dots**), λem: 640–700 nm (Mitotracker red).

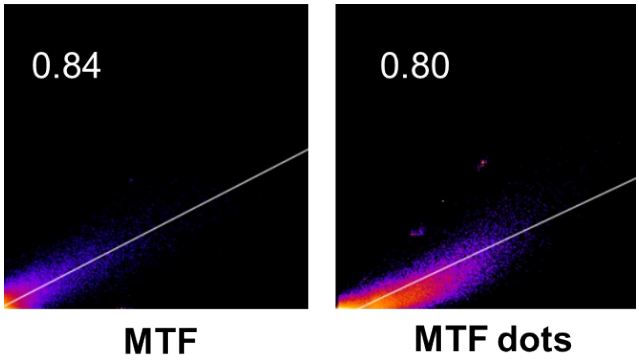

Fig. S16 Colocalization scatterplots of **MTF** (Pearson Correlation Coefficient = 0.84) and **MTF dots** (Pearson Correlation Coefficient = 0.80), respectively.

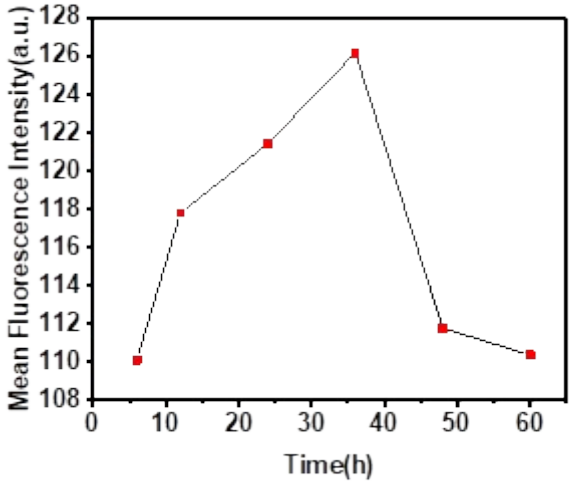

Fig. S17 The mean fluorescence intensity curve of tumors after **MTF dots** injection.

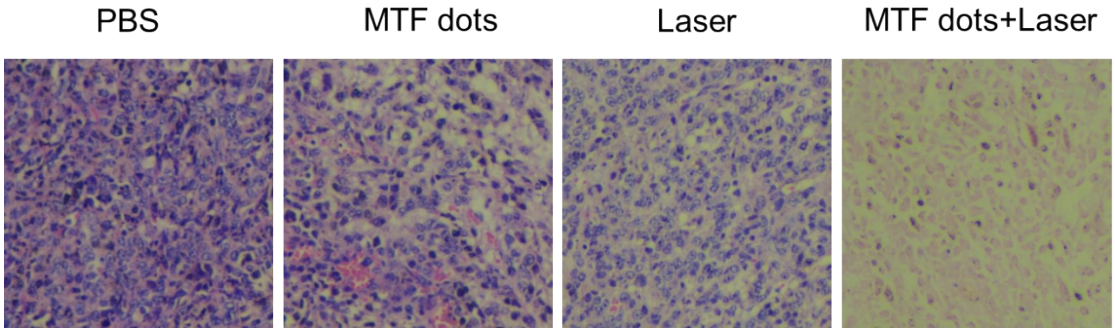

Fig. S18 H&E staining of tumors in different groups.

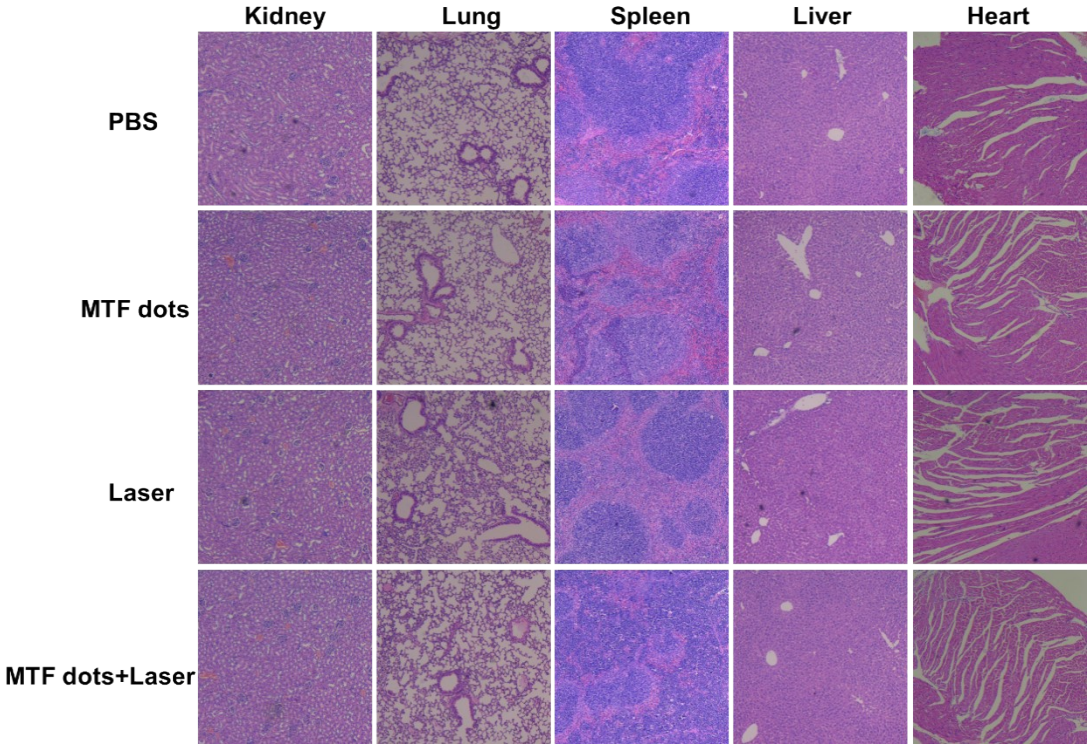

Fig. S19 H&E staining of different organs in different groups.

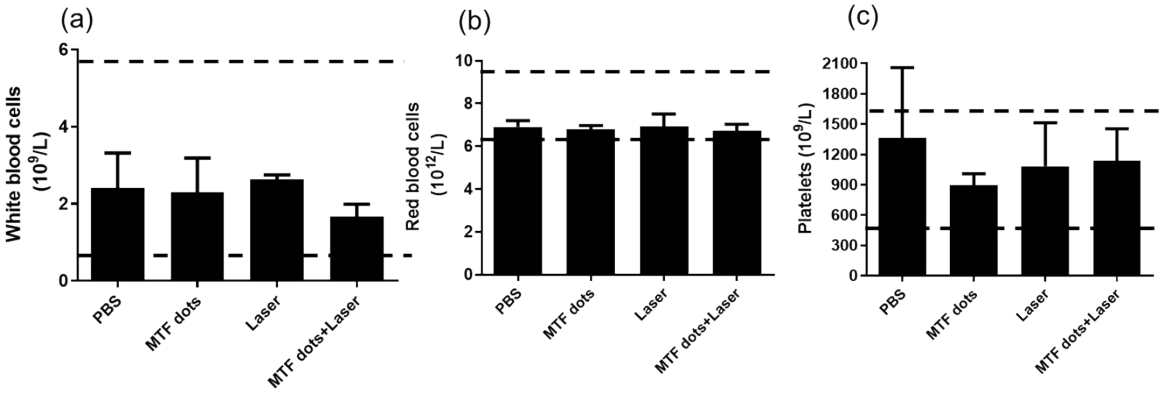

Fig. S20 Major blood cells in different groups treated with different conditions.

References

1. B. Ding, Y. Xiao, H. Zhou, X. Zhang, C. Qu, F. Xu, Z. Deng, Z. Cheng and X. Hong, *J. Med. Chem.*, 2019, **62**, 2049-2059.
2. H. Zhou, X. Zeng, A. Li, W. Zhou, L. Tang, W. Hu, Q. Fan, X. Meng, H. Deng, L. Duan, Y. Li, Z. Deng, X. Hong and Y. Xiao, *Nat. Commun.*, 2020, **11**, 6183.
3. T. Yang, L. Liu, Y. Deng, Z. Guo, G. Zhang, Z. Ge, H. Ke and H. Chen, *Adv. Mater.* 2017, **29**, 1700487.
4. G. Hong, Y. Zou, A. L. Antaris, S. Diao, D. Wu, K. Cheng, X. Zhang, C. Chen, B. Liu and Y. He, J. Wu, J. Yuan, B. Zhang, Z. Tao, C. Fukunaga and H, Dai, *Nat. Commun.*, 2014, **5**, 4206.